Yi et al. *EPJ Quantum Technology* (2025) 12:43
https://doi.org/10.1140/epjqt/s40507-025-00347-0

EPJ Quantum Technology
a SpringerOpen Journal

EPJ.org

RESEARCH Open Access

A probabilistic quantum algorithm for imaginary-time evolution based on Taylor expansion

Xin Yi[1], Jiacheng Huo[2], Guanhua Liu[3], Ling Fan[4,5], Ru Zhang[2,5,6] and Cong Cao[4,5,6*]

*Correspondence:
caocong@bupt.edu.cn
[4]School of Electronic Engineering, Beijing University of Posts and Telecommunications, Beijing, 100876, China
[5]Beijing Key Laboratory of Space-Ground Interconnection and Convergence, Beijing University of Posts and Telecommunications, Beijing, 100876, China
Full list of author information is available at the end of the article

Abstract

Imaginary-time evolution is a powerful tool for obtaining the ground state of a quantum system, but the complexity of classical algorithms designed for simulating imaginary-time evolution will increase significantly as the size of the quantum system becomes larger. Here, a probabilistic quantum algorithm based on Taylor expansion for implementing imaginary-time evolution is introduced. For Hamiltonians composed of Pauli product terms, the quantum circuit requires only a single ancillary qubit and is exclusively constructed using elementary single-qubit and two-qubit gates. Furthermore, similar principles are used to extend the algorithm to the case where the Hamiltonian takes a more general form. The algorithm only requires negligible precomputed numerical calculations, without the need for complex classical pre-mathematical calculations or optimization loops. We demonstrate the algorithm by solving the ground state energy of hydrogen molecules and Heisenberg Hamiltonians. Moreover, we conducted experiments on real quantum computers through the quantum cloud platform to find the ground state energy of Heisenberg Hamiltonians. Our work extends the methods for realizing imaginary-time evolution on quantum computers, and our algorithm exhibits potential for implementation on near-term quantum devices, particularly when the Hamiltonian consists of Pauli product terms.

Keywords: Quantum algorithm; Linear combination of unitaries; Imaginary-time evolution; Ground state simulation

1 Introduction

Imaginary-time evolution (ITE), functioning as a mathematical tool, has exerted a significant influence on various conundrums within quantum physics. This encompasses tasks like resolving the ground state of a Hamiltonian [1–17], analyzing properties at finite temperatures [9, 18], simulating dynamics in real-time [19, 20], and executing quantum simulations for non-Hermitian systems [21, 22]. Utilizing a classical computer, we have the capability to simulate imaginary-time evolution through the evaluation of the propagator, subsequently applying it to the wave function of the system. Furthermore, a range of associated classical techniques are available, including quantum Monte Carlo [20, 23, 24],

Springer

density matrix renormalization group [25, 26], and tensor networks [27]. However, the dimension of the Hilbert space experiences exponential growth in tandem with the scale of the quantum system, rendering the tasks unmanageable for classical computers [28].

The quantum computer stands as a promising instrument for the efficient simulation of quantum systems [29–31]. However, realizing the ITE operation on a quantum computer is not as straightforward as its counterpart on a classical computer, owing to the non-unitary nature of ITE [32]. This characteristic renders a direct implementation through a sequence of elementary quantum gates impossible. There are primarily three indirect but practical methods to implement ITE on a quantum computer. The first method known as variational ITE (VITE) [5–7, 33, 34] employs the framework of variational quantum algorithms. Initially, it addresses the optimization parameters of a unitary ansatz using McLachlan's variational principle on a classical computer [35]. Subsequently, the parameters within the ansatz circuit are refined to generate a converged state, approximating the actual ground state [36]. The second method, known as quantum ITE (QITE) [8–10, 37, 38], employs classical methods to solve the linear equation. Subsequently, it embarks on a variational quest to identify a unitary process that provides a close approximation to the exact evolved states. The third method, known as probabilistic ITE (PITE) [12–14, 39–41], exploits measurements to implement non-unitary operations. Through the application of unitary operations within the expanded Hilbert space, one can achieve the intended final state within a specific subspace of the ancillary qubits.

The three types of ITE mentioned above are not necessarily mutually exclusive. In fact, there are mathematical connections between VITE and QITE, and a combination of QITE and PITE was proposed recently [42]. Nonetheless, each of these methods presents its own limitations. For instance, classical optimizers within VITE might exhibit slow convergence and struggle to fully exploit the computational capabilities of quantum computers. QITE involves intricate precomputed mathematical processes, whereas PITE requires the execution of iterative circuits, each of which must be applied successfully. Therefore, designing new quantum approaches to implement imaginary-time evolution, with the aim of minimizing the aforementioned drawbacks, becomes particularly important.

In this paper, we propose a probabilistic quantum algorithm for implementing imaginary-time evolution based on Taylor expansion. In the proposed algorithm, when the Hamiltonian consists of Pauli product terms, which is the most general and significant case. The imaginary-time evolution operator in each Trotter step can be approximated by a linear combination of an identity operator and a Pauli product operator through Taylor expansion. This can be achieved using the technique of linear combination of unitaries (LCU) with only one ancillary qubit [43–45]. The quantum circuit is composed entirely of elementary single-qubit and two-qubit gates, which is highly compatible with quantum devices in the NISQ era. Furthermore, we extend the algorithm to cases where the Hamiltonian takes a more general form. The algorithm only requires negligible precomputed numerical calculations, without the need for complex classical pre-mathematical calculations or optimization loops. Numerical simulations are conducted to solve the ground states of hydrogen molecular Hamiltonians and Heisenberg Hamiltonians. We also analyze the complexity and success probability of the algorithm and provide a method for enhancing the success probability. Experiments on real quantum computers via a cloud platform are used to further validate the feasibility of the algorithms. Our work extends the methods for realizing imaginary-time evolution on quantum computers. When the

Hamiltonian consists of Pauli-product terms, our algorithm has the potential to be implemented on near-term quantum devices.

This paper is organized as follows. In Sect. 2, we give a description of the TTITE algorithm. Section 3 shows some numerical simulation results. In Sect. 4, we analyze the Trotter decomposition error and the Taylor expansion error. Section 5 analyzes the complexity and proposes a method to improve the success probability. In Sect. 6, we discuss the generalized TTITE algorithm in the case where Hamiltonian is not composed of Pauli terms. We show some experimental results on the quantum cloud platform in Sect. 7.

2 Method

2.1 Imaginary-time evolution

Imaginary-time evolution serves as a mathematical tool commonly employed to numerically determine highly accurate approximations to the ground state. The concept of imaginary-time evolution can be understood as follows: by defining the imaginary-time, $\tau = it$, and substituting it into the Schrodinger equation $i\hbar\frac{d|\psi\rangle}{dt} = H|\psi\rangle$, where H represents a hermitian Hamiltonian, we obtain the imaginary-time Schrodinger equation

$$-\frac{d|\psi\rangle}{d\tau} = H|\psi\rangle. \tag{1}$$

Given an initial state $|\psi(0)\rangle$, we denote the solution to Eq. (1) as $|\psi(\tau)\rangle = A(\tau)e^{-H\tau}|\psi(0)\rangle$, where $e^{-H\tau}$ represents a non-unitary evolution operator, and $A(\tau) = 1/\sqrt{\langle\psi(0)|e^{-2H\tau}|\psi(0)\rangle}$ serves as a normalization parameter. Assuming that the initial state $|\psi(0)\rangle$ is not orthogonal to the ground state of the Hamiltonian H, a sufficiently long imaginary-time evolution will result in the state at imaginary-time τ closely approximating the ground state of the Hamiltonian H.

In the context of implementing imaginary-time evolution, classical methods face exponential growth in computational resources required as the system size increases. Therefore, it is natural to consider the quantum version of the imaginary-time evolution algorithm as a solution to overcome these exponential bottlenecks. The realization of the imaginary-time evolution on quantum circuits relies on the precise implementation of the aforementioned non-unitary evolution operator $e^{-H\tau}$.

2.2 Trotter-Taylor imaginary-time evolution (TTITE)

For an n-qubit Hamiltonian $H = \sum_{i=1}^{m} c_i h_i$ composed of Pauli product terms, where c_i represents real coefficients in the linear combination, $h_i = \otimes_{j=1}^{n}\sigma_\alpha^j$ denotes the Pauli product terms, and σ_α^j represents either a Pauli matrix or an identity matrix acting on the j-th qubit, with $\alpha \in \{0, x, y, z\}$ (we adopt the notation $\sigma_0 = I$).

Our objective is to execute the non-unitary operator $e^{-H\tau}$ on quantum circuits. To accomplish this, we begin by employing the Trotter approximation [46, 47] to decompose the imaginary-time propagator into

$$e^{-H\tau} = \left(e^{-c_1 h_1 \Delta\tau}\cdots e^{-c_m h_m \Delta\tau}\right)^{\frac{\tau}{\Delta\tau}} + O(\Delta\tau). \tag{2}$$

For the sake of descriptive convenience, we refer to $S(\Delta\tau) = \left(e^{-c_1 h_1 \Delta\tau}\cdots e^{-c_m h_m \Delta\tau}\right)$ as a Trotter segment and $T_i(\Delta\tau) = e^{-c_i h_i \Delta\tau}$ as a Trotter step. After a single Trotter step, a quan-

tum state $|\psi\rangle$ is transformed as follows (after normalization):

$$\left|\psi'\right\rangle = e^{-c_i h_i \Delta\tau} |\psi\rangle . \tag{3}$$

$T_i(\Delta\tau)$ remains a non-unitary operator. The realization of the non-unitary operator $T_i(\Delta\tau)$ has become the key to implementing non-unitary imaginary-time propagator $e^{-H\tau}$.

A matrix exponential, resembling $T_i(\Delta\tau)$, can be defined using a Taylor series expansion. Consequently, $T_i(\Delta\tau)$ satisfies the following equation:

$$T_i(\Delta\tau) \approx T_i^R(\Delta\tau) = \sum_{j=0}^{R} \frac{(-c_i\Delta\tau)^j}{j!} h_i^j, \tag{4}$$

where $T_i^R(\Delta\tau)$ denotes the R-order Taylor expansion. Due to the fact that, when j is even, $h_i^j = I$, and when j is odd, $h_i^j = h_i$. Equation (4) can be rewritten as:

$$T_i(\Delta\tau) \approx T_i^R(\Delta\tau) = \alpha I + \beta h_i, \tag{5}$$

where $\alpha = \sum_{j=0,j=even}^{R} \frac{(-c_i\Delta\tau)^j}{j!}$ and $\beta = \sum_{k=0,k=odd}^{R} \frac{(-c_i\Delta\tau)^k}{k!}$. When $R \to \infty$, $T_i(\Delta\tau) = T_i^R(\Delta\tau)$.

In order to realize the non-unitary operation $T_i(\Delta\tau)$ in a quantum circuit, we add an ancillary qubit $|0\rangle$. The scheme is based on the linear combination of unitaries, which is a technique widely used in algorithm design [43, 44, 48]. Algorithm 1 and Fig. 1(a) outline the realization of a Trotter step $T_i(\Delta\tau)$ in the TTITE algorithm, with details of each step as follows:

Step 1: the encoding of the ancillary and work systems. For the n-qubit work system, the initial state is $|\psi\rangle$, which needs to have a finite overlap with the ground state. For the one-qubit ancillary system, the encoding process is realized by a single-qubit gate $R_y(\theta)$ acting on the state $|0\rangle$, where $\theta = 2\arccos\left(\frac{\alpha}{\sqrt{\alpha^2+\beta^2}}\right)$. We denote the whole state of the composite

Algorithm 1 Trotter step $T_i(\Delta\tau)$ for the TTITE algorithm

Input: the state $|\psi\rangle$, the Trotter segment duration $\Delta\tau$, the coefficient c_i, the Pauli product term h_i, and the Taylor expansion order R.
Output: the state $\left|\psi'\right\rangle$.
Step 1 Initialize the ancillary and the work systems to the state
$|\phi_1\rangle = \left(\frac{\alpha}{\sqrt{\alpha^2+\beta^2}}|0\rangle + \frac{\beta}{\sqrt{\alpha^2+\beta^2}}|1\rangle\right)|\psi\rangle$,
where $\alpha = \sum_{j=0,j=even}^{R} \frac{(-c_i\Delta\tau)^j}{j!}$ and $\beta = \sum_{k=0,k=odd}^{R} \frac{(-c_i\Delta\tau)^k}{k!}$.
Step 2 Apply the controlled unitary $CU = |0\rangle\langle 0| \otimes I_{2^n} + |1\rangle\langle 1| \otimes h_i$ on both the work and ancillary registers. We obtain
$|\phi_2\rangle = \frac{1}{\sqrt{\alpha^2+\beta^2}}(\alpha|0\rangle|\psi\rangle + \beta|1\rangle h_i|\psi\rangle)$.
Step 3 Perform the Hadamard operation on the ancillary qubit. The state of the whole system becomes
$|\phi_3\rangle = \frac{1}{\sqrt{2(\alpha^2+\beta^2)}}[|0\rangle(\alpha I + \beta h_i)|\psi\rangle + |1\rangle(\alpha I - \beta h_i)|\psi\rangle]$.
Step 4 Measure the ancillary qubit. If the result is $|0\rangle$, we successfully obtain the state
$|\phi_4\rangle = \frac{1}{\|(\alpha I+\beta h_i)|\psi\rangle\|}[|0\rangle(\alpha I + \beta h_i)|\psi\rangle]$.
Readout: The output state of the work system is $\left|\psi'\right\rangle$.

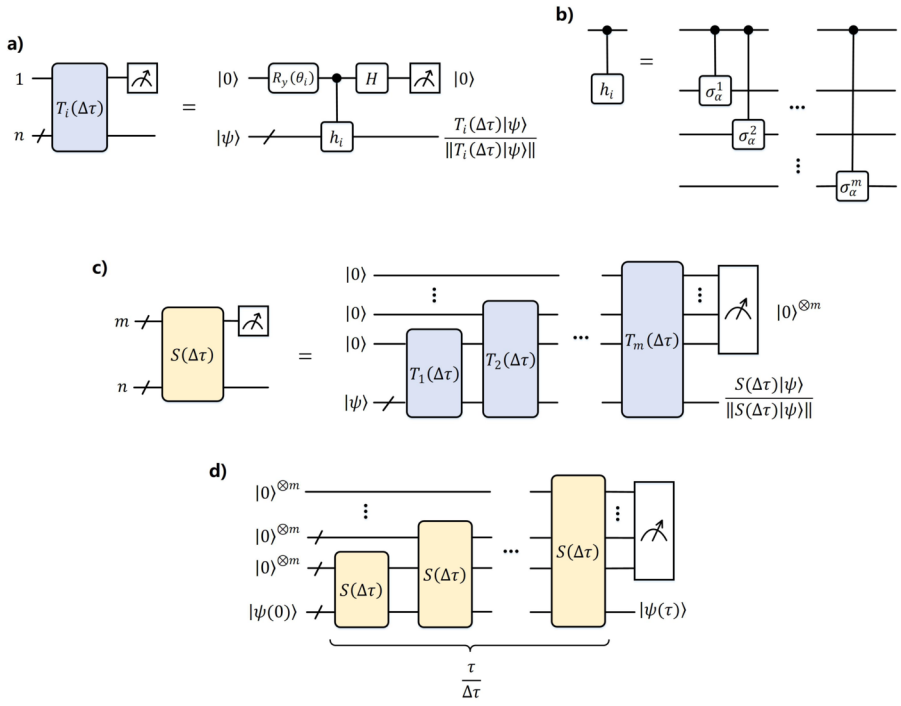

Figure 1 *Quantum circuit for implementing TTITE.* **a)** Element component of quantum circuit for implementing $T_i(\Delta\tau)$. $|\psi\rangle$ and $|0\rangle$ denote the initial state of the work and ancillary systems, respectively. The controlled operation that acted on the work system are *CU* in Eq. (7). At the end of the circuit, we measure the final state of the ancillary system. If the ancillary qubit is $|0\rangle$, the work system collapses into state $|\psi'\rangle$. **b)** The explicit form of the operation *CU*. σ_α^j represents Pauli matrix or 2×2 identity matrix acting on the jth qubit. **c)** Modular quantum circuits for the realization of $S(\Delta\tau)$. **d)** Modular quantum circuits for the realization of $e^{-H\tau}$

system as

$$|\phi_1\rangle = \left(\frac{\alpha}{\sqrt{\alpha^2+\beta^2}} |0\rangle + \frac{\beta}{\sqrt{\alpha^2+\beta^2}} |1\rangle \right) |\psi\rangle . \tag{6}$$

Step 2: this part introduces an ancillary qubit-controlled unitary operation *CU* to entangle the ancillary and work systems. Here,

$$CU = |0\rangle\langle 0| \otimes I_{2^n} + |1\rangle\langle 1| \otimes h_i, \tag{7}$$

where I_{2^n} is the $2^n \times 2^n$ identity matrix. Afterward, the ancillary and work qubits are entangled, and state $|\phi_1\rangle$ is transformed into

$$|\phi_2\rangle = \frac{1}{\sqrt{\alpha^2+\beta^2}} (\alpha |0\rangle |\psi\rangle + \beta |1\rangle h_i |\psi\rangle) . \tag{8}$$

In fact, *CU* can be further simplified into several one-qubit-controlled Pauli operators, as shown in Fig. 1(b).

Step 3: a Hadamard gate is performed on the ancillary qubit. The state of the whole system becomes

$$|\phi_3\rangle = \frac{1}{\sqrt{2\left(\alpha^2+\beta^2\right)}}\left[|0\rangle\left(\alpha I+\beta h_i\right)|\psi\rangle + |1\rangle\left(\alpha I-\beta h_i\right)|\psi\rangle\right]. \tag{9}$$

Step 4: finally, the ancillary qubit is measured. If the ancillary qubit is $|0\rangle$, we successfully obtain the state

$$|\phi_4\rangle = \frac{1}{\|\left(\alpha I+\beta h_i\right)|\psi\rangle\|}\left[|0\rangle\left(\alpha I+\beta h_i\right)|\psi\rangle\right], \tag{10}$$

and the work system is in the state $\left|\psi'\right\rangle = T_i(\Delta\tau)|\psi\rangle$. The success probability of obtaining $|0\rangle$ in the measurement is given by

$$P_s = \frac{1}{2\left(\alpha^2+\beta^2\right)}\|T_i(\Delta\tau)|\psi\rangle\|^2. \tag{11}$$

To avoid repetitive measurements for state reconstruction and the repeated execution of the initial state preparation procedure for the work system, we can embed the circuit in Fig. 1(a) as a primitive circuit within a larger quantum system. In Fig. 1(c), the ancillary systems include m qubits with the same process as above and the composite quantum system includes $m+n$ qubits. After measuring the ancillary system and obtaining a state of $|0\rangle^{\otimes m}$, the state of the work system is $\frac{S(\Delta\tau)|\psi\rangle}{\|S(\Delta\tau)|\psi\rangle\|}$, which is equivalent to the initial state $|\psi\rangle$ evolved over a Trotter segment denoted by $S(\Delta\tau)$ (after normalization).

Similarly, multiple Trotter segments in the Trotter expansion can be employed using similar methods as described above, at the expense of augmenting the number of ancillary qubits, shown in Fig. 1(d). This approach effectively reduces the resource consumption attributed to repetitive measurements and initial state preparation. If all the ancillary qubits are $|0\rangle$, we can directly get the target quantum state $|\psi(\tau)\rangle = A(\tau)e^{-H\tau}|\psi(0)\rangle$ in the work system, which is an approximation to the ground state of Hamiltonian H.

3 Numerical simulation

To demonstrate the correctness and performance of the algorithm, we conducted numerical simulations to solve the ground state and ground-state energy of two physical systems: the hydrogen molecule and the Heisenberg Hamiltonian.

3.1 Hydrogen molecule

To tackle the task of determining the ground state and ground-state energy of H_2 on a quantum computer [49], we employ the STO-3G basis set and employ the Jordan-Wigner transformation [50, 51]. This approach allows us to derive Hamiltonians consisting of Pauli matrices $H_{H_2} = \sum_i c_i(D)\sigma_\alpha^1\cdots\sigma_\alpha^n$, which can be implemented on n qubits, with the coefficients $c_i(D)$ being dependent on the interatomic distance D. Consequently, the Hamiltonian for H_2 can be effectively encoded onto 4 qubits [41]. Subsequently, further mapping is applied to compactly encode the H_2 Hamiltonian onto 2 qubits (see details in Ref. [52]), resulting in the H_2 Hamiltonian taking the form of

$$H_{H_2} = c_0(D) + c_1(D)\sigma_z^1 + c_2(D)\sigma_z^2 + c_3(D)\sigma_z^1\sigma_z^2 + c_4(D)\sigma_x^1\sigma_x^2, \tag{12}$$

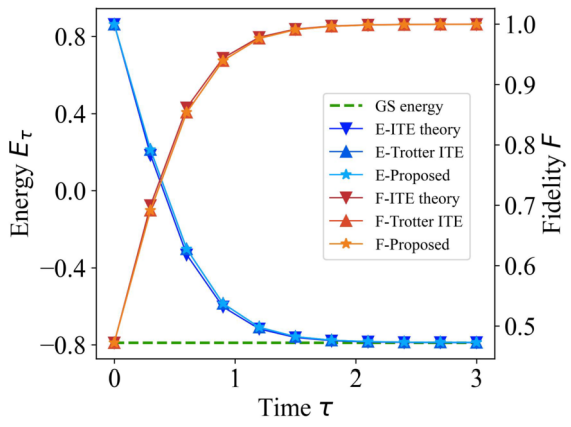

Figure 2 *Numerical simulation results for the ground state of the hydrogen molecule with $D = 0.35$ Å.* Captions "E-ITE theory", "E-Trotter ITE", and "E-Proposed"depict the convergence of energy E_τ, with "E-ITE theory"representing the theoretical results of ITE, "E-Trotter ITE"representing the theoretical results of ITE under Trotter decomposition, and "E-Proposed"representing the results of the proposed algorithm under a 5th-order Taylor expansion. Similarly, Captions "F-ITE theory", "F-Trotter ITE", and "F-Proposed"illustrate the variations in fidelity F

where the coefficients at different D are available in the supplementary information of Ref. [52].

In numerical simulations, we use 1 qubit as an ancillary system and 2 qubits as work systems to represent the H_2 molecule. We begin by conducting a numerical simulation at a fixed atomic distance of $D = 0.35$ Å. The initial state is chosen as $|+\rangle|+\rangle$, and the total imaginary-time evolution duration is $\tau = 3$, with a Trotter segment duration of $\Delta\tau = 0.3$. Energy $E_\tau = \langle\psi(\tau)|H|\psi(\tau)\rangle$ and fidelity $F\left(|\psi(\tau)\rangle, |gs\rangle\right) = \sqrt{\left|\langle\psi(\tau)|gs\rangle\right|^2}$ where $|gs\rangle$ represents the ground state of Hamiltonian H, are two metrics used to evaluate the performance of the algorithm. The variation of energy E_τ and fidelity F with imaginary-time evolution time τ is shown in Fig. 2. The results of the proposed algorithm are compared with the theoretical results of the imaginary-time evolution and the theoretical results of the imaginary-time evolution under Trotter decomposition. In this case, the proposed algorithm performs a 5th-order Taylor expansion (expansion to the 4th term) in each Trotter step. As the evolution time τ increases, after 10 evolution steps, the energy E_τ converges to the exact value, the fidelity F rises to 1, and the proposed algorithm closely aligns with the theoretical situation.

To obtain the most stable molecular structure, we vary the interatomic distance to map the potential energy surface of the H_2 molecule, as shown in Fig. 3. The initial state is chosen as $\frac{4}{\sqrt{19}}|00\rangle + \frac{1}{\sqrt{19}}|01\rangle + \frac{1}{\sqrt{19}}|10\rangle + \frac{1}{\sqrt{19}}|11\rangle$, and the Trotter segment duration is still $\Delta\tau = 0.3$. We analyze the performance of the proposed algorithm for 2nd and 10th-order Taylor expansions (expansions to 1st and 9th-order terms) in each Trotter step. The result ($\tau = 0.3$, $\tau = 1.2$, $\tau = 3$) are compared with the initial state energies ($\tau = 0$) and the ground-state energies obtained by diagonalization. The results show that for each Trotter step, the Taylor expansion to the 2nd and 10th order is always effective, which indicates that our algorithm only needs to perform a low-order Taylor expansion to achieve a good approximation (even if a higher-order expansion is required, it only adds some trivial classical computations). Besides, the lowest energy of the potential energy surface corresponds to the interatomic distance of about 0.75 Å, which is consistent with the theoretical value.

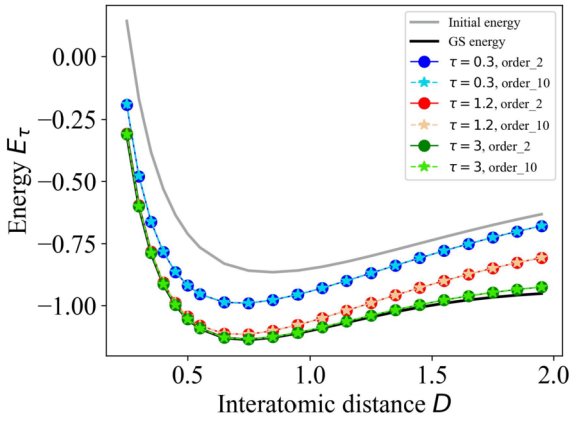

Figure 3 H_2 *energy as a function of* τ *and the interatomic distance D.* Captions "$\tau = 0.3$, order_2"and "$\tau = 0.3$, order_10"respectively depict the H_2 energy after imaginary-time evolution at $\tau = 0.3$ using the proposed algorithm with 2nd and 10th-order Taylor expansions, under different interatomic distances. The remaining captions have similar implications

3.2 Heisenberg spin-1/2 chain Hamiltonian

We then consider the following Heisenberg spin-1/2 chain Hamiltonian with open boundaries,

$$H_{Heisenberg} = -J\sum_{j=1}^{n-1}\left(\sigma_x^j\sigma_x^{j+1} + \sigma_y^j\sigma_y^{j+1} + \sigma_z^j\sigma_z^{j+1}\right) - h\sum_{j=1}^{n}\sigma_z^j, \tag{13}$$

where J is the coupling strength and h is the static magnetic field [53]. We first perform numerical simulations with the Heisenberg model with $n = 6$ and $J = h = 1$. The initial state is chosen as $|+\rangle^{\otimes 6}$, and the total imaginary-time evolution duration is $\tau = 2$, with a Trotter segment duration of $\Delta\tau = 0.1$. In Fig. 4, we show the variation of energy E_τ and fidelity F with evolution time τ. The results demonstrate an alignment between the outcomes of the proposed algorithm and the theoretical results obtained from the Trotter decomposition-based imaginary-time evolution, which also shows that the discrepancies between the outcomes of the proposed algorithm and the theoretical results of the imaginary-time evolution are mainly caused by the Trotter decomposition. Furthermore, the results of the proposed algorithm with 2nd and 10th-order expansions (expansions to 1st and 9th-order terms) at each single Trotter step are also in good agreement, which again shows that our algorithm needs only a low Taylor expansion order to achieve high accuracy.

To study the performance of the algorithm at different problem sizes, we perform numerical simulations with the Heisenberg model with $n = 3, 6, 9, 12$ for the case of $J = h = 1$. For each problem size, the initial state is chosen as $|+\rangle^{\otimes n}$, and the total imaginary-time evolution duration is $\tau = 2$, with a Trotter segment duration of $\Delta\tau = 0.1$. At each single Trotter step, a 5th-order Taylor expansion (expansion to the 4th term) is applied. For comparison purposes, the normalized energy $NE_\tau = \frac{E_\tau - E_{min}}{E_{max} - E_{min}}$ is used to scale the different energies E_τ to the interval $[0, 1]$. E_{min} and E_{max} are the minimum and maximum energy of the Hamiltonian, respectively, which are calculated exactly. $NE_\tau = 0$ corresponds to the energy E_τ as the ground state energy. The results in Fig. 5 show that in all cases, the normalized energy NE_τ converges to 0 and the fidelity F increases to 1 as the evolution time

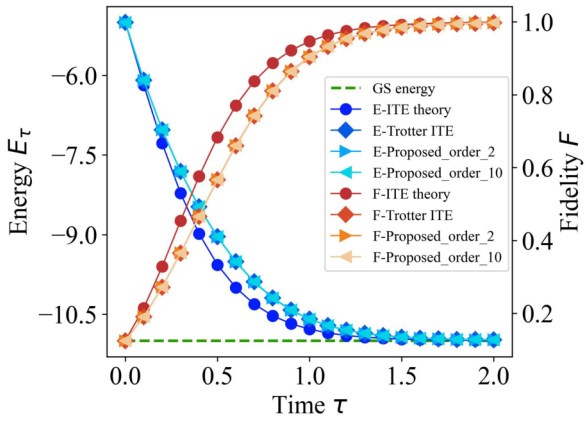

Figure 4 *Numerical simulation results for the Heisenberg ground state with $n = 6$ and $J = h = 1$.* Captions "E-ITE theory", "E-Trotter ITE", "E-Proposed_order_2", and "E-Proposed_order_10"depict the convergence of energy E_τ, with "E-ITE theory"representing the theoretical results of ITE, "E-Trotter ITE"representing the theoretical results of ITE under Trotter decomposition, "E-Proposed_order_2"and "E-Proposed_order_10"representing the results of the proposed algorithm under a 2nd and 10th-order Taylor expansion. Similarly, Captions "F-ITE theory", "F-Trotter ITE", "F-Proposed_order_2", and "F-Proposed_order_10"illustrate the variations in fidelity F

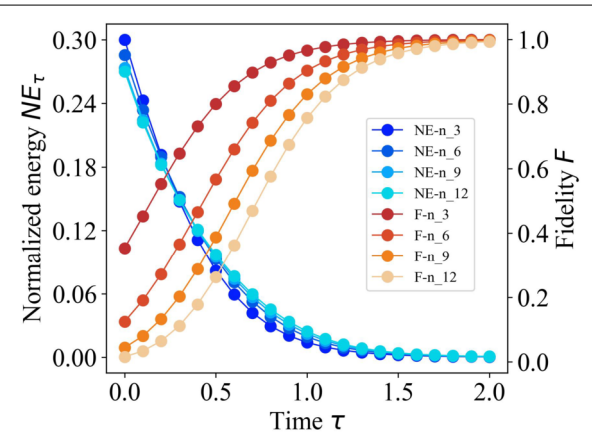

Figure 5 *Numerical simulation results for the Heisenberg ground state at different scales for $J = 1$, $h = 1$.* Captions "NE-n_3", "NE-n_6", "NE-n_9", and "NE-n_12"represent the convergence of normalized energy NE_τ for $n = 3$, $n = 6$, $n = 9$, and $n = 12$, respectively. Similarly, Captions "F-n_3", "F-n_6", "F-n_9", and "F-n_12"illustrate the variations in fidelity F

increases. The proposed algorithm maintains the validity of the ground state solution despite the exponential growth of the dimensionality of the Hamiltonian quantities.

4 Error analysis

Here we provide a detailed analysis of the impact of the Trotter decomposition error and Taylor expansion error on the algorithm. We begin by examining the disparity between the corresponding imaginary-time evolution operator $e^{-H_{random}\tau}$ and the Taylor expansion approximation operator $T^R(\tau) = \sum_{j=0}^{R} \frac{(-\tau)^j}{j!} H^j_{random}$, using a random Hamiltonian H_{random} consisting of a tensor product of 6 Pauli operators as an example. We define the similarity between operators A and B in terms of cosine similarity $cs(A,B) = \frac{A \cdot B}{\|A\| \cdot \|B\|}$, and the disparity between operators A and B as $\epsilon(A,B) = 1 - cs(A,B)$. Figure 6(a) illustrates the error

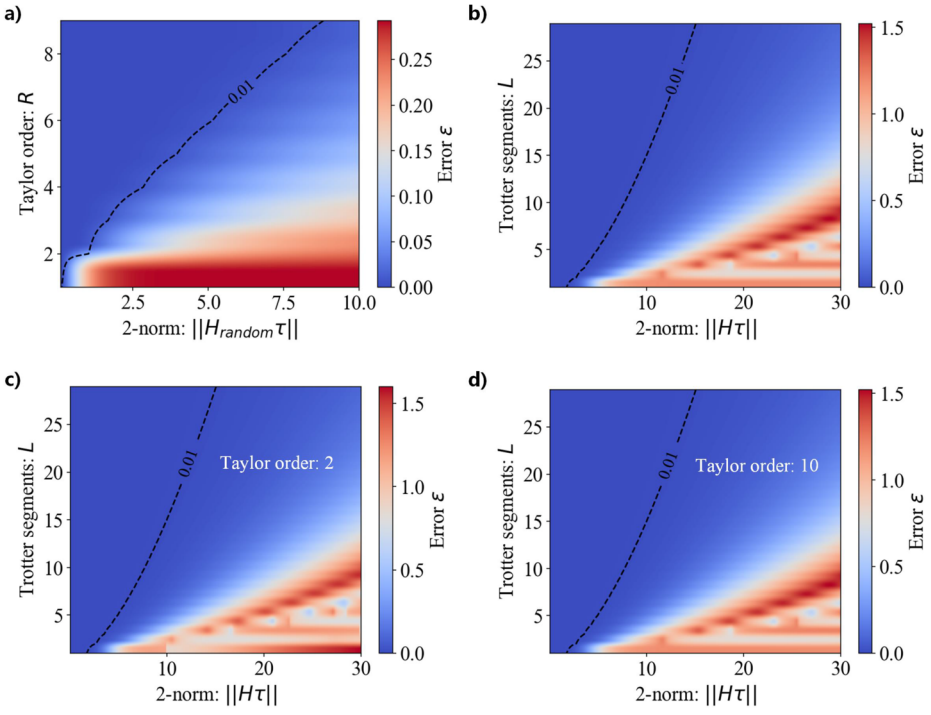

Figure 6 *Analysis of Taylor expansion error and Trotter decomposition error.* **a)** The error map of $\epsilon\left(e^{-H_{random}\tau}, T^R(\tau)\right)$, where H_{random} is a random Hamiltonian consisting of a tensor product of 6 Pauli operators. The labeled dashed lines form a low-error area with $\epsilon \leq 0.01$. **b)** The error map of $\epsilon\left(e^{-H_{Heisenberg}\tau}, S(\Delta\tau)^L\right)$, where $H_{Heisenberg}$ is a Heisenberg Hamiltonian with $n = 6$, $J = 1.37$ and $h = 0.23$. **c)** The error map of $\epsilon\left(e^{-H_{Heisenberg}\tau}, S(\Delta\tau)_2{}^L\right)$. **d)** The error map of $\epsilon\left(e^{-H_{Heisenberg}\tau}, S(\Delta\tau)_{10}{}^L\right)$

$\epsilon\left(e^{-H_{random}\tau}, T^R(\tau)\right)$ and its relation with parameters R and $\|H_{random}\tau\|$, where R is the Taylor expansion order and $\|H_{random}\tau\|$ is the 2-norm. As the imaginary-time τ increases, it is observed that a linear growth of R is sufficient to ensure a satisfactory approximation (error $\epsilon = 0.01$) between the Taylor expansion approximation operator and the imaginary-time evolution operator. This indicates that we do not require a significant amount of classical resources in order to achieve a high-quality approximation of the corresponding imaginary-time evolution operator.

We further investigate the impact of Trotter decomposition error on the algorithm. Taking the example of a Heisenberg Hamiltonian with $n = 6$, $J = 1.37$ and $h = 0.23$, we examine the error between the imaginary-time evolution operator $e^{-H_{Heisenberg}\tau}$ and the Trotter decomposition operator $S(\Delta\tau)^L$, where $\Delta\tau = \tau/L$. Figure 6(b) illustrates the error $\epsilon\left(e^{-H_{Heisenberg}\tau}, S(\Delta\tau)^L\right)$ and its relation with parameters L and $\left\|H_{Heisenberg}\tau\right\|$, where L is the number of Trotter decomposition segments. Finally, we conduct a comprehensive analysis of the combined impact of the Trotter decomposition error and Taylor expansion error on the algorithm. Specifically, for each Trotter step $T_i(\Delta\tau)$ in the Trotter segment $S(\Delta\tau)$, we perform second-order and 10th-order Taylor expansions. That is $S(\Delta\tau)_2 = \prod_i T_i^2(\Delta\tau)$ and $S(\Delta\tau)_{10} = \prod_i T_i^{10}(\Delta\tau)$. Figure 6(c) illustrates the error $\epsilon\left(e^{-H_{Heisenberg}\tau}, S(\Delta\tau)_2{}^L\right)$ and its relation with parameters L and $\left\|H_{Heisenberg}\tau\right\|$. Figure 6(d) illustrates the error $\epsilon\left(e^{-H_{Heisenberg}\tau}, S(\Delta\tau)_{10}{}^L\right)$ and its relation with parameters L and $\left\|H_{Heisenberg}\tau\right\|$. The error maps of Fig. 6(c) and Fig. 6(d) are almost identical to the er-

ror map of Fig. 6(b), indicating that the errors in the algorithm primarily come from the Trotter decomposition. This also reiterates that a low-order Taylor expansion can provide a high level of approximation accuracy.

In summary, the error introduced by the Taylor expansion has a negligible impact on the performance of the algorithm and requires only minimal classical computational resources. In contrast, the Trotter decomposition error is the primary source of inaccuracy, requiring a careful balance between computational precision and resource consumption. Nevertheless, since Trotter decomposition error is a well-known challenge in algorithms that employ Trotterization and has been extensively studied, existing research can be leveraged to further improve performance.

5 Performance and complexity analysis

We analyzed the performance and complexity of the algorithm in four aspects: qubit resources, gate complexity, evolutionary efficiency, and measurement probability. For qubit resources, the implementation of operator $e^{-c_i h_i \Delta\tau}$ requires the introduction of an ancillary qubit. Therefore, we need $n + mL$ qubits for an m-term Hamiltonian in total, where $L = \tau/\Delta\tau$ is the number of Trotter segment. For gate complexity, the operator $e^{-c_i h_i \Delta\tau}$ can be decomposed into $O(n)$ basic gates, and a total of $O(nmL)$ basic gates are needed for an m-term Hamiltonian.

Next, we must determine the parameter L. Alternatively, we need to ascertain the value of τ when $\Delta\tau$ is provided. It is crucial to do this before proceeding with the algorithm to avoid measuring the expectation values during the algorithm procedure. Such measurements could destroy the state of the work qubits and halt the algorithm. To determine L, we demonstrate that after the evolution of imaginary-time τ, the square of the fidelity between $|\psi(\tau)\rangle$ and the exact ground state $|E_0\rangle$ is restricted to

$$F^2\left(|\psi(\tau)\rangle, |E_0\rangle\right) \leq \frac{|a_0|^2}{|a_0|^2 + \left(1 - |a_0|^2\right) e^{-2\tau\Omega_{max}}}, \tag{14}$$

where $|a_0|^2$ is the initial fidelity at $\tau = 0$, Ω_{max} is the gap between the highest excited state and the ground state (see Appendix A for proof). When the square of the fidelity between $|\psi(\tau)\rangle$ and $|E_0\rangle$ is greater than $1 - e$, the imaginary-time length

$$\tau = O\left(\frac{1}{\Omega_{max}} log \frac{1}{e}\right), \tag{15}$$

is linearly dependent on the inverse of the energy gap of Hamiltonian, and logarithmically dependent on the inverse of output error. In the above analysis, we did not take into account the errors caused by Trotter decomposition, which can be reduced by utilizing higher-order Trotter decompositions, such as

$$e^{-H\tau} = \left[\left(e^{-c_1 h_1 \frac{\Delta\tau}{2}} \cdots e^{-c_m h_m \frac{\Delta\tau}{2}}\right) \times \left(e^{-c_1 h_1 \frac{\Delta\tau}{2}} \cdots e^{-c_m h_m \frac{\Delta\tau}{2}}\right)\right]^{\frac{\tau}{\Delta\tau}} + O\left(\Delta\tau^2\right). \tag{16}$$

We also analyze the success probability of our algorithm, and Lemma 1 below gives that the success probability $P(s \cdot \Delta\tau)$ of our algorithm in each Trotter segment does not exponentially decrease to zero with the increasing imaginary-time τ. Instead, the success

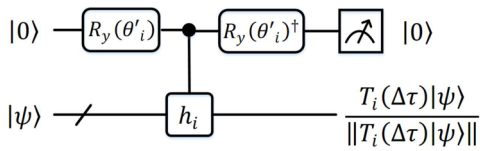

Figure 7 Improved circuits for enhancing the success probability of the TTITE algorithm

probability of each Trotter segment is monotonically increasing. Here, the success probability $P(s \cdot \Delta\tau)$ corresponds to the measurement result when we have obtained the state $|\psi\left((s-1)\Delta\tau\right)\rangle$ (see Appendix B for proof).

Lemma 1 *The success probability of each Trotter segment is an increasing sequence such that*

$$P(\Delta\tau) \leq P(2\Delta\tau) \leq \cdots \leq P(L\Delta\tau). \tag{17}$$

To further improve the success probability of the algorithm, we can make slight adjustments to the quantum circuit. For each Trotter step, which corresponds to implementing the operator $e^{-c_i h_i \Delta\tau}$, we modify the $R_y(\theta)$ gate to $R_y(\theta')$ in Step 1 of Algorithm 1, where $\theta' = 2\arccos\left(\sqrt{\frac{\alpha}{\alpha+\beta}}\right)$. As a result, the state of the composite system changes from $|\phi_1\rangle$ to

$$\left|\phi_1'\right\rangle = \left(\sqrt{\frac{\alpha}{\alpha+\beta}}\,|0\rangle + \sqrt{\frac{\beta}{\alpha+\beta}}\,|1\rangle\right)|\psi\rangle\,. \tag{18}$$

In addition, we replace the Hadamard gate in Step 3 with a $R_y(\theta')^\dagger$ gate, and the state of the composite system changes from $|\phi_3\rangle$ to

$$\left|\phi_3'\right\rangle = \frac{1}{\alpha+\beta}\left[|0\rangle\left(\alpha I + \beta h_i\right)|\psi\rangle + |1\rangle\left(-\sqrt{\alpha\beta}I + \sqrt{\alpha\beta}h_i\right)|\psi\rangle\right]. \tag{19}$$

Similarly, if the ancillary qubit is $|0\rangle$, the work system is in the state $T_i(\Delta\tau)\,|\psi\rangle$. The corresponding quantum circuit diagram is shown in Fig. 7. The success probability of obtaining $|0\rangle$ in the measurement is given by

$$P_s' = \frac{1}{(\alpha+\beta)^2}\|T_i(\Delta\tau)\,|\psi\rangle\|^2. \tag{20}$$

Obviously, due to the fact that $(\alpha+\beta)^2 \leq 2\left(\alpha^2+\beta^2\right)$, we obtain $P_s' \geq P_s$.

We studied the success probability of the algorithm using the example of solving the ground state of the hydrogen molecule with $D = 0.25$ Å, and the results are shown in Fig. 8.

6 Generalization of algorithm

In this section, we aim to extend the TTITE algorithm to encompass scenarios where the Hamiltonian is not restricted to being a sum of Pauli terms. In general, the Hamiltonian is written as $H = \sum_{i=1}^{m} H[i]$, and the imaginary-time operator is decomposed into

$$e^{-H\tau} = \left(e^{-H[1]\Delta\tau}\cdots e^{-H[m]\Delta\tau}\right)^{\frac{\tau}{\Delta\tau}} + O(\Delta\tau). \tag{21}$$

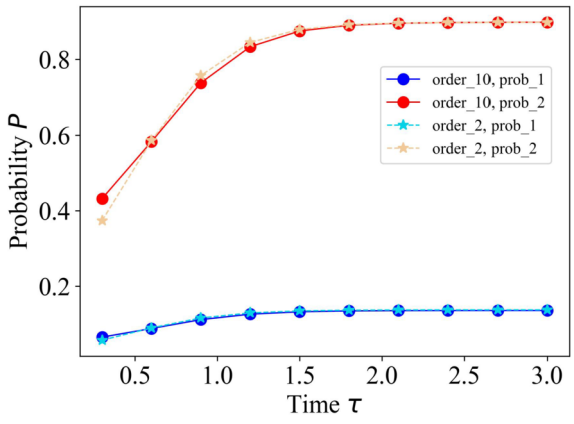

Figure 8 *Analysis of probability.* Captions "order_10, prob_1"and "order_10, prob_2"represent the success probabilities of the circuits in Fig. 1(a) and Fig. 7 under a 10th-order Taylor expansion. Captions "order_2, prob_1"and "order_2, prob_2"represent the success probabilities of the circuits in Fig. 1(a) and Fig. 7 under a 2nd-order Taylor expansion

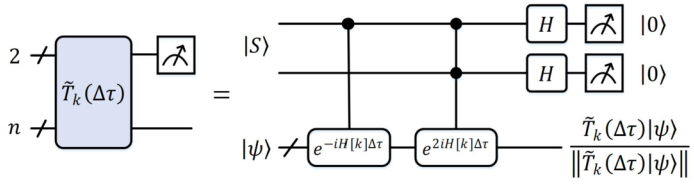

Figure 9 *Quantum circuit for implementing* $\widetilde{T}_k(\Delta\tau)$. $|\psi\rangle$ and $|S\rangle$ denote the initial state of the work and ancillary systems, respectively. At the end of the circuit, we measure the final state of the ancillary system. If all the ancillary qubits are $|0\rangle$, the work system collapses into state $\frac{\widetilde{T}_k(\Delta\tau)|\psi\rangle}{\|\widetilde{T}_k(\Delta\tau)|\psi\rangle\|}$

For a Trotter step $\widetilde{T}_k(\Delta\tau) = e^{-H[k]\Delta\tau}$, we can approximate it as

$$e^{-H[k]\Delta\tau} = 2I + \alpha^- e^{-iH[k]\Delta\tau} + \alpha^+ e^{iH[k]\Delta\tau} + O(\Delta\tau^3), \tag{22}$$

where $\alpha^- = -(1+i)/2$ and $\alpha^+ = -(1-i)/2$ (see Appendix C for proof). Obviously, the form of Eq. (22) is a linear combination of some unitary operations, and we can implement the operator $\widetilde{T}_k(\Delta\tau)$ on a quantum circuit in Fig. 9 with the following steps:

Step a: the initialization of the ancillary and work system. Specifically, the work system is initialized to $|\psi\rangle$ and the ancillary system is initialized to $\frac{1}{\sqrt{3}}(|00\rangle + |01\rangle + \alpha^- |10\rangle + \alpha^+ |11\rangle)$. We denote the state of the composite system as

$$|\widetilde{\phi}_1\rangle = \frac{1}{\sqrt{3}}\left(|00\rangle + |01\rangle + \alpha^- |10\rangle + \alpha^+ |11\rangle\right)|\psi\rangle\,. \tag{23}$$

Step b: two controlled unitary operators are introduced to entangle the ancillary and work systems. The first operator $|0\rangle\langle 0|_1 \bigotimes I_{2^n} + |1\rangle\langle 1|_1 \bigotimes e^{-iH[k]\Delta\tau}$ is a 1-controlled unitary evolution, controlled by the first ancillary qubit. The second one is a two-qubit controlled operator, if both ancillary qubits are in state $|1\rangle$, unitary operator $e^{2iH[k]\Delta\tau}$ will be

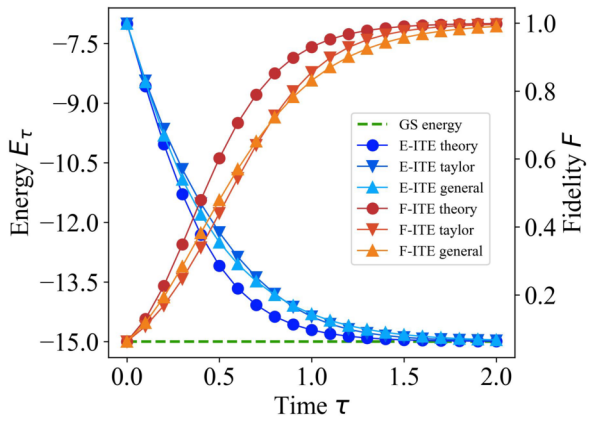

Figure 10 *Numerical simulation results for Generalized TTITE algorithm.* Captions "E-ITE theory", "E-ITE taylor", and "E-ITE general"depict the convergence of energy E_τ, with "E-ITE theory"representing the theoretical results of ITE, "E-ITE taylor"representing the results of TTITE under 5th-order Taylor expansion, and "E-ITE general"representing the results of generalized TTITE. Similarly, Captions "F-ITE theory", "F-ITE taylor", and "F-ITE general"illustrate the variations in fidelity F

applied to the work system. The state $|\widetilde{\phi}_1\rangle$ is transformed into

$$|\widetilde{\phi}_2\rangle = \frac{1}{\sqrt{3}}\left(|00\rangle|\psi\rangle + |01\rangle|\psi\rangle + \alpha^-|10\rangle e^{-iH[k]\Delta\tau}|\psi\rangle + \alpha^+|11\rangle e^{iH[k]\Delta\tau}|\psi\rangle\right). \tag{24}$$

Step c: Hadamard gates are performed on both ancillary qubits and then the ancillary system is measured. If both the ancillary qubits are $|0\rangle$, we successfully obtain the state

$$|\widetilde{\phi}_3\rangle = \mathbb{N}\left[|00\rangle\left(2I + \alpha^- e^{-iH[k]\Delta\tau} + \alpha^+ e^{iH[k]\Delta\tau}\right)|\psi\rangle\right], \tag{25}$$

where $\mathbb{N}$ is the normalization parameter.

We apply the generalized TTITE to the simulations of the Heisenberg Hamiltonian with $n = 8$ and $J = h = 1$. Instead of taking $c_i h_i$ as $H[i]$, we consider $-J\left(\sigma_x^j\sigma_x^{j+1} + \sigma_y^j\sigma_y^{j+1} + \sigma_z^j\sigma_z^{j+1}\right)$ (where $j = 1, \ldots, n-1$) as $H[p]$ (where $p = 1, \ldots, n-1$) and $-h\sum_{j=1}^{n}\sigma_z^j$ as $H[n]$. As shown in Fig. 10, the results of the generalized TTITE algorithm are compared with the theoretical results of the imaginary-time evolution and the results of the TTITE algorithm under 5th-order Taylor expansion. The results indicate that the generalized TTITE algorithm and the TTITE algorithm exhibit similar performance, effectively addressing the ground state problem.

7 Experimental results

We further verify the correctness of the proposed algorithm by conducting experiments on a real quantum computer through the quantum cloud platform. Our results are based on the "Quafu"open cloud platform, which provides three superconducting quantum processors, namely ScQ-10, ScQ-18, and ScQ-136. Specifically, we take a Heisenberg Hamiltonian with $n = 2$, $J = 1$ and $h = 5$ as an example. The two-qubit Heisenberg Hamiltonian contains 5 non-identity terms, each corresponding to a non-unitary evolution operator when we apply the algorithm,

$$\widetilde{Q}_1 = \exp\left(h\sigma_x^1\Delta\tau\right),$$

$$\widetilde{Q}_2 = \exp\left(h\sigma_x^2 \Delta\tau\right),$$
$$\widetilde{Q}_3 = \exp\left(J\sigma_x^1\sigma_x^2 \Delta\tau\right),$$
$$\widetilde{Q}_4 = \exp\left(J\sigma_y^1\sigma_y^2 \Delta\tau\right),$$
$$\widetilde{Q}_5 = \exp\left(J\sigma_z^1\sigma_z^2 \Delta\tau\right).$$

For each Trotter segment, we select $\Delta\tau = 0.02$, and for each non-unitary evolution operator, we perform a 10th-order Taylor expansion. In the experiments, we need to apply $\widetilde{Q}_1$, $\widetilde{Q}_2$, $\widetilde{Q}_3$, $\widetilde{Q}_4$, $\widetilde{Q}_5$ on the work system in turn, as a cycle. At the end of each iteration, we need to measure the expected value of energy to demonstrate the convergence of the algorithm. The quantum circuits used to implement $\widetilde{Q}_k$ ($k = 1, 2, 3, 4, 5$) is shown in Fig. 11. These circuits consist of the following four parts, corresponding to steps 1 to 4 in Algorithm 1:

(1) The blue blocks correspond to step 1 in Algorithm 1 for the initial encoding of the ancillary and work systems. As the state of the work system only evolves in the real-coefficient subspace spanned by $|00\rangle$ and $|11\rangle$, the preparation only requires a $R_y(\beta)$ gate and a *CNOT* gate. The angular parameter of $R_y(\beta)$ can be obtained from the tomography and measurement results of the previous quantum circuit. For the first Trotter step, the input state of the work system is $\frac{1}{\sqrt{2}}(|00\rangle + |11\rangle)$, which can be achieved by replacing $R_y(\beta)$ gate with Hadamard gate.

(2) The yellow blocks correspond to step 2 in Algorithm 1 for entangling the ancillary and work systems.

(3) The green blocks correspond to step 3 in Algorithm 1.

(4) The red blocks correspond to step 4 in Algorithm 1 for measurement. For each quantum circuit, we conduct experiments on three superconducting quantum processors, ScQ-10, ScQ-18, and ScQ-136. Each quantum processor performs 50,000 measurements to eliminate the effect of noise. After the measurement of the $\widetilde{Q}_5$ circuit, we calculate the expected value of energy.

In Fig. 11(f), the experimental results of the "Quafu"quantum cloud platform overlap well with the theoretical results, confirming the feasibility of the algorithm.

8 Discussion and conclusion

The PITE algorithm proposed in this paper, TTITE, can effectively prepare the ground state of a Hamiltonian, making it highly significant in both physical implications and practical applications. The PITE algorithm overcomes several limitations present in recent methods. For instance, it avoids the classical bottleneck caused by classical optimization loops in certain VITE algorithms and the accuracy constraints imposed by fixed ansatz. Moreover, it eliminates the restrictions on Hamiltonian locality and the need for complex precomputed mathematical operations found in some QITE algorithms. Compared to similar PITE algorithms, when the Hamiltonian consists of Pauli product terms, the proposed TTITE algorithm eliminates the need for relatively complex controlled $e^{-iH\Delta t}$ operations, as required in Ref. [12, 40], and instead relies on fundamental single-qubit rotation gates and two-qubit gates, thereby simplifying the quantum circuit. Additionally, unlike the method in Ref. [14, 40], which introduces multiple ancillary qubits, TTITE requires only a single ancillary qubit, effectively reducing quantum resource consumption. Furthermore, it avoids the reliance on computationally intensive classical operations such

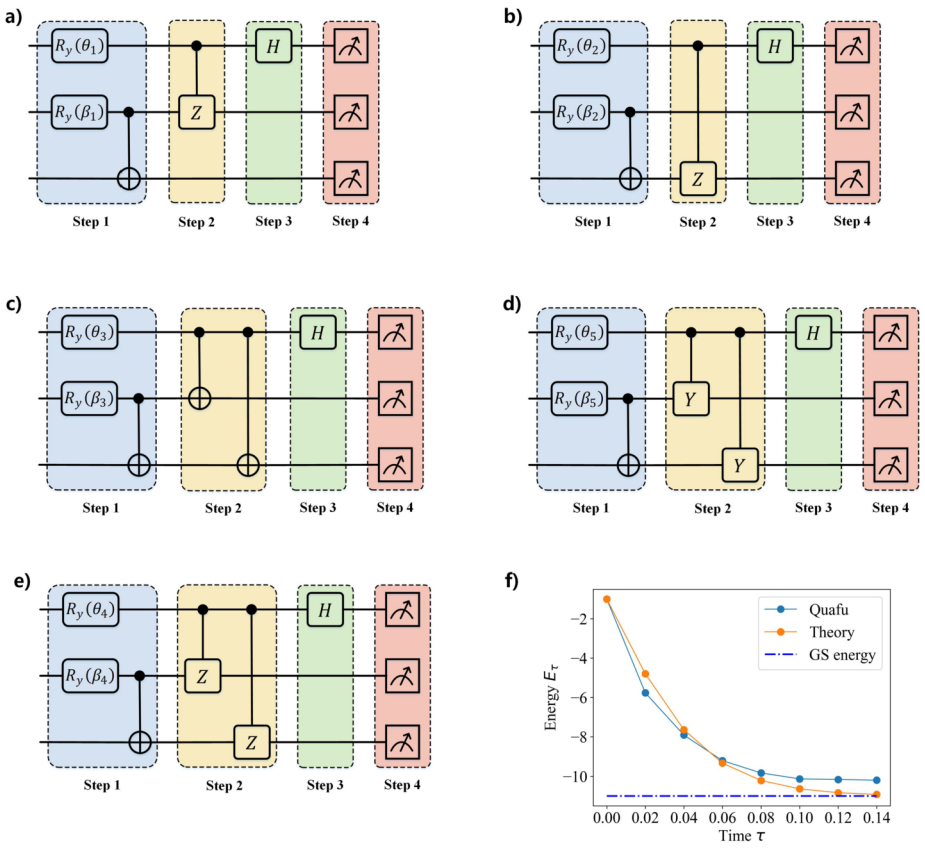

Figure 11 *Cloud platform experimental circuits and results.* Steps 1-4 correspond to the steps in Algorithm 1. **a)** Quantum circuit for $\widetilde{Q}_1$. **b)** Quantum circuit for $\widetilde{Q}_2$. **c)** Quantum circuit for $\widetilde{Q}_3$. **d)** Quantum circuit for $\widetilde{Q}_4$. **e)** Quantum circuit for $\widetilde{Q}_5$. **f)** Results for "Quafu"quantum cloud platform

as singular value decomposition, as seen in Ref. [13, 14], and instead requires only a negligible Taylor series expansion, significantly improving the efficiency of the algorithm.

A major limitation of PITE-type algorithms, including the one proposed in this paper, is that the total success probability decreases exponentially as the number of Trotter segments increases. Although we have demonstrated that the success probability of each individual Trotter segment increases with the evolution time, the exponential decline in the total success probability remains unavoidable. This issue involves a trade-off between algorithm accuracy and resource consumption. For a fixed imaginary-time evolution duration τ, a larger Trotter segment $\Delta\tau$ results in fewer total steps, which is beneficial for both success probability and resource efficiency. However, this also leads to a larger Trotter error, potentially compromising algorithm accuracy. Conversely, a smaller Trotter segment $\Delta\tau$ reduces the Trotter error and ensures higher accuracy but requires more steps, leading to lower success probability and higher resource consumption. Such trade-offs are a common challenge in many quantum algorithms that rely on Trotter decomposition.

We have proposed a method to improve the success probability of Trotter segment by making only simple modifications to the quantum circuit structure. In addition to this approach, several other methods can also enhance the success probability: 1) Amplitude amplification techniques can be incorporated after the quantum circuit of each Trotter segment to boost the success probability, as demonstrated in Ref. [14, 54]. 2) The total

success probability largely depends on the required imaginary-time evolution duration τ for convergence to the ground state. This duration is primarily influenced by two factors: Intrinsic properties of the system, such as the energy gap between the ground state and the first excited state, which is difficult to modify. Choice of the initial state. Selecting an initial state with good overlap with the ground state can significantly reduce the required evolution time τ. In this work, the chosen initial states exhibit relatively poor overlap, but using improved initial states, such as the Hartree-Fock (HF) state, could lead to better performance. 3) Reducing Trotter error can also improve the success probability. Trotter error is determined by the intrinsic complexity of the Hamiltonian. For instance, when many non-commuting terms are applied sequentially, the error increases. If the Hamiltonian contains a large number of commuting terms, optimizing the ordering of local terms can maximize the number of commuting partitions [55, 56]. Additionally, a randomized ordering of Hamiltonian terms can be considered to mitigate Trotter error [57].

Future research will focus on further exploring methods and techniques to enhance the success probability of the algorithm, investigating its convergence behavior across a wider range of scenarios and larger problem instances, and analyzing the effects of noise on its performance.

In conclusion, we have proposed a probabilistic quantum algorithm based on Taylor expansion for implementing imaginary-time evolution. When the Hamiltonian is composed of Pauli product terms, the quantum circuit requires the introduction of only one ancillary qubit and is entirely composed of fundamental single-qubit and two-qubit gates. This demonstrates the potential of the proposed algorithm for implementation on near-term quantum devices. Furthermore, we generalize the algorithm to address more general cases, where the Hamiltonian is not composed of Pauli product terms. We demonstrated the performance and feasibility of the algorithm with numerical simulations and experiments using hydrogen molecules and Heisenberg Hamiltonians as examples. We also analyzed the complexity and success probability of the algorithm and provided precise methods for enhancing the success probability. Error analysis conducted on the algorithm indicates that, during the simulation of imaginary-time evolution, the Trotter decomposition error constitutes the primary source of inaccuracies. The introduced errors from the Taylor expansion are minimal and can be enhanced through straightforward classical computations. Our work extends the methods for realizing imaginary-time evolution on quantum computers, with the potential for implementation on near-term quantum devices under specific conditions.

Appendix A: Derivation of output fidelity and analysis of evolutionary efficiency

In general, the Hamiltonian of a quantum system is Hermitian, and its eigenvalues are all real numbers. Consider an N-dimensional system, assuming that the eigenvalues and eigenvectors are $\{(E_i, |E_i\rangle)\}_{i=0}^{N-1}$, and the eigenvalues are sorted as $E_0 \leq E_1 \leq \cdots \leq E_{N-1}$. The initial state $|\psi(0)\rangle$ can be represented as a linear expansion of eigenstates

$$|\psi(0)\rangle = \sum_{i=0}^{N-1} a_i |E_i\rangle . \tag{A.1}$$

After the evolution under the imaginary-time τ, the state $|\psi(0)\rangle$ becomes

$$|\psi(\tau)\rangle = \frac{e^{-H\tau}|\psi(0)\rangle}{\sqrt{\langle\psi(0)|e^{-2H\tau}|\psi(0)\rangle}}. \tag{A.2}$$

The square of the fidelity between $|\psi(\tau)\rangle$ and the ground state $|E_0\rangle$ is

$$\begin{aligned} F^2\left(|\psi(\tau)\rangle, |E_0\rangle\right) &= |\langle\psi(\tau)|E_0\rangle|^2 \\ &= \frac{\langle\psi(0)|e^{-H\tau}|E_0\rangle\langle E_0|e^{-H\tau}|\psi(0)\rangle}{\langle\psi(0)|e^{-2H\tau}|\psi(0)\rangle} \\ &= \frac{|a_0|^2 e^{-2E_0\tau}}{\sum_{i=0}^{N-1}|a_i|^2 e^{-2E_i\tau}} \\ &= \frac{|a_0|^2}{|a_0|^2 + \sum_{i=1}^{N-1}|a_i|^2 e^{-2\tau(E_i-E_0)}}. \end{aligned} \tag{A.3}$$

Defining $E_i - E_0 = \Omega_i$. It is evident that $\Omega_i < \Omega_{N-1}$ and $\sum_{i=0}^{N-1}|a_i|^2 = 1$, thus we have:

$$F^2 \leq \frac{|a_0|^2}{|a_0|^2 + \left(1-|a_0|^2\right)e^{-2\tau\Omega_{N-1}}}. \tag{A.4}$$

Furthermore, we can find the relation between the imaginary-time length τ and the output fidelity error $e = 1 - F^2$:

$$\tau \geq \frac{1}{2\Omega_{N-1}} ln\left(\frac{1-e}{e}\frac{1-|a_0|^2}{|a_0|^2}\right). \tag{A.5}$$

So the imaginary-time length τ is linearly dependent on the inverse of the energy gap of Hamiltonian, and logarithmically dependent on the inverse of output error.

Appendix B: Derivation of the increasing property of success probability

As shown in the main text, a Trotter segment is $S(\Delta\tau) = T_m(\Delta\tau)\cdots T_1(\Delta\tau)$, where $T_i(\Delta\tau) = e^{-c_i h_i \Delta\tau} = \alpha_i I + \beta_i h_i$, $\alpha_i = \sum_{j=0,j=even}^{\infty}\frac{(-c_i\Delta\tau)^j}{j!}$ and $\beta_i = \sum_{j=0,j=odd}^{\infty}\frac{(-c_i\Delta\tau)^j}{j!}$. The success probability of each Trotter segment is

$$P[(s+1)\Delta\tau] = \frac{1}{\mathbb{C}}\|T_m(\Delta\tau)\cdots T_1(\Delta\tau)|\psi(s\Delta\tau)\rangle\|^2, \tag{B.1}$$

where $\mathbb{C} = \sqrt{2^m\left({\alpha_1}^2 + {\beta_1}^2\right)\cdots\left({\alpha_m}^2 + {\beta_m}^2\right)}$. After making a measurement, we get the state $|\psi((s+1)\Delta\tau)\rangle$ with probability $P[(s+1)\Delta\tau]$.

By the same trick, the success probability of obtaining state $|\psi((s+2)\Delta\tau)\rangle$ is given by

$$P[(s+2)\Delta\tau] = \frac{1}{\mathbb{C}}\|T_m(\Delta\tau)\cdots T_1(\Delta\tau)|\psi((s+1)\Delta\tau)\rangle\|^2. \tag{B.2}$$

According to the Trotter theorem, we know that when $\Delta\tau$ is small enough, we have $T_m(\Delta\tau)\cdots T_1(\Delta\tau) \approx e^{-H\Delta\tau}$. Therefore, Eq. (B.1) and Eq. (B.2) can be approximated as:

$$P[(s+2)\Delta\tau] = \frac{1}{\mathbb{C}}\left\|e^{-H\Delta\tau}|\psi((s+1)\Delta\tau)\rangle\right\|^2,$$

$$P[(s+1)\,\Delta\tau] = \frac{1}{\mathbb{C}}\left\| e^{-H\Delta\tau}\,|\psi\,(s\Delta\tau)\rangle \right\|^2.$$

State $|\psi\,(s\Delta\tau)\rangle$ and $|\psi\,((s+1)\,\Delta\tau)\rangle$ can be represented as linear combinations of eigenstates, namely $|\psi\,(s\Delta\tau)\rangle = \sum_{i=0}^{N-1} a_i^s\,|E_i\rangle$ and $|\psi\,((s+1)\,\Delta\tau)\rangle = \sum_{i=0}^{N-1} a_i^{s+1}\,|E_i\rangle$, where $\sum_{i=0}^{N-1}\left|a_i^s\right|^2 = 1$ and $\sum_{i=0}^{N-1}\left|a_i^{s+1}\right|^2 = 1$.

We now show $P[(s+2)\,\Delta\tau] \geq P[(s+1)\,\Delta\tau]$ by showing $\frac{P[(s+2)\Delta\tau]}{P[(s+1)\Delta\tau]} \geq 1$. That is

$$\begin{aligned}\frac{P[(s+2)\,\Delta\tau]}{P[(s+1)\,\Delta\tau]} &= \frac{\left\| e^{-H\Delta\tau}\,|\psi\,((s+1)\,\Delta\tau)\rangle \right\|^2}{\left\| e^{-H\Delta\tau}\,|\psi\,(s\Delta\tau)\rangle \right\|^2} \\ &= \frac{\sum_{i=0}^{N-1}\left|a_i^{s+1}\right|^2 e^{-2E_i\Delta\tau}}{\sum_{i=0}^{N-1}\left|a_i^{s}\right|^2 e^{-2E_i\Delta\tau}} \\ &= \frac{\sum_{i=0}^{N-1}\left|a_i^{s}\right|^2 e^{-4E_i\Delta\tau}}{\left(\sum_{i=0}^{N-1}\left|a_i^{s}\right|^2 e^{-2E_i\Delta\tau}\right)^2}. \end{aligned} \tag{B.3}$$

By using the inequality $e^{-2E_i\Delta\tau} \geq e^{-2E_j\Delta\tau}$ for $i < j$, we have

$$\begin{aligned}&\sum_{i=0}^{N-1}\left|a_i^{s}\right|^2 e^{-4E_i\Delta\tau} - \left(\sum_{i=0}^{N-1}\left|a_i^{s}\right|^2 e^{-2E_i\Delta\tau}\right)^2 \\ &= \sum_{i,j=0}^{N-1} e^{-4E_i\Delta\tau}\left|a_i^s\right|^2\left|a_j^s\right|^2 - \sum_{i,j=0}^{N-1} e^{-2E_i\Delta\tau}\left|a_i^s\right|^2 e^{-2E_j\Delta\tau}\left|a_j^s\right|^2 \\ &= \sum_{i,j=0}^{N-1} e^{-2E_i\Delta\tau}\left(e^{-2E_i\Delta\tau} - e^{-2E_j\Delta\tau}\right)\left|a_i^s\right|^2\left|a_j^s\right|^2 \\ &= \sum_{i=0}^{N-1}\sum_{j=i+1}^{N-1}\left(e^{-2E_i\Delta\tau} - e^{-2E_j\Delta\tau}\right)^2\left|a_i^s\right|^2\left|a_j^s\right|^2 \geq 0. \end{aligned} \tag{B.4}$$

Therefore, we obtain $\frac{P[(s+2)\Delta\tau]}{P[(s+1)\Delta\tau]} \geq 1$.

Next, we derive $P(L\Delta\tau)$, where $L = \tau/\Delta\tau$. That is

$$P(L\Delta\tau) = \frac{1}{\mathbb{C}}\left\| e^{-H\Delta\tau}\,|\psi\,((L-1)\Delta\tau)\rangle \right\|^2. \tag{B.5}$$

Since at the L-th Trotter segment, the state is essentially converged to the ground state, $|\psi\,((L-1)\Delta\tau)\rangle \approx |E_0\rangle$. We have

$$P(L\Delta\tau) = \frac{1}{\mathbb{C}}\left\| e^{-H\Delta\tau}\,|E_0\rangle \right\|^2 = \frac{e^{-2E_0\Delta\tau}}{\mathbb{C}}. \tag{B.6}$$

Appendix C: General expansion derivation of $e^{-H\tau}$

According to the Taylor expansion of the matrix exponential, the non-unitary imaginary-time evolution operator $e^{-H\tau}$ can be expressed as

$$e^{-H\tau} = I - A + A^2 - A^3 + A^4 - A^5 + A^6 - A^7 + A^8 - \cdots,$$

where $A^j = \frac{\tau^j}{j!}H^j$. In the same way, two unitary operators representing forward and backward time evolution can also be expanded as

$$e^{iH\tau} = I + iA + (-1)A^2 + (-i)A^3 + A^4 + \cdots,$$
$$e^{-iH\tau} = I + (-i)A + (-1)A^2 + iA^3 + A^4 + \cdots.$$

Then we can rewrite the non-unitary imaginary-time operator as

$$e^{-H\tau} = 2I + \alpha^- e^{-iH\tau} + \alpha^+ e^{iH\tau} + O(\tau^3), \tag{C.1}$$

which is a linear combination of three unitary operators.

Abbreviations
ITE, imaginary-time evolution; VITE, variational imaginary-time evolution; QITE, quantum imaginary-time evolution; PITE, probabilistic imaginary-time evolution; LCU, linear combination of unitaries; NISQ, noisy intermediate-scale quantum; TTITE, Trotter-Taylor imaginary-time evolution.

Acknowledgements
Thanks for the support from the China Mobile project "Key Technologies and Core Capabilities for Quantum Computing" (Project No. R24113G5C06).

Author contributions
XY contributed to the idea and wrote the main manuscript text. JH and GL participated in the discussions and performed data curation. LF, RZ and CC improved the manuscript and supervvised the research. All authors read and approved the final manuscript.

Funding information
The work was supported by Fund of State Key Laboratory of Information Photonics and Optical Communications (Beijing University of Posts and Telecommunications) (No. IPOC2022ZT07), P. R. China. This work was also supported by the National Natural Science Foundation of China (NSFC) under Grant Nos. 61701035 and 61671085.

Data availability
No datasets were generated or analysed during the current study.

Materials availability
Not applicable.

Code availability
Not applicable.

Declarations

Ethics approval and consent to participate
Not applicable.

Consent for publication
The Author confirms: that the work described has not been published before; that it is not under consideration for publication elsewhere; that its publication has been approved by all co-authors.

Competing interests
The authors declare no competing interests.

Author details
[1]Future Research Laboratory, China Mobile Research Institute, Beijing, 100053, China. [2]School of Science, Beijing University of Posts and Telecommunications, Beijing, 100876, China. [3]School of Transportation, Beijing Jiaotong University, Beijing, 100044, China. [4]School of Electronic Engineering, Beijing University of Posts and Telecommunications, Beijing, 100876, China. [5]Beijing Key Laboratory of Space-Ground Interconnection and Convergence, Beijing University of Posts and Telecommunications, Beijing, 100876, China. [6]State Key Laboratory of Information Photonics and Optical Communications, Beijing University of Posts and Telecommunications, Beijing, 100876, China.

Received: 20 August 2024 Accepted: 27 March 2025 Published online: 03 April 2025

References

1. Lehtovaara L, Toivanen J, Eloranta J. Solution of time-independent Schrodinger equation by the imaginary time propagation method. J Comput Phys. 2007;221(1):148–57.
2. Kraus CV, Generalized CJI. Hartree-Fock theory for interacting fermions in lattices: numerical methods. New J Phys. 2010;12(11):113004.
3. Turro F, Roggero A, Amitrano V, et al. Imaginary-time propagation on a quantum chip. Phys Rev A. 2022;105(2):022440.
4. McClean JR, Aspuru-Guzik A. Compact wavefunctions from compressed imaginary time evolution. RSC Adv. 2015;5(124):102277–83.
5. McArdle S, Jones T, Endo S, et al. Variational ansatz-based quantum simulation of imaginary time evolution. npj Quantum Inf. 2019;5(1):75.
6. Jones T, Endo S, McArdle S, et al. Variational quantum algorithms for discovering Hamiltonian spectra. Phys Rev A. 2019;99(6):062304.
7. Yuan X, Endo S, Zhao Q, et al. Theory of variational quantum simulation. Quantum. 2019;3:191.
8. Yeter-Aydeniz K, Pooser RC, Siopsis G. Practical quantum computation of chemical and nuclear energy levels using quantum imaginary time evolution and Lanczos algorithms. npj Quantum Inf. 2020;6(1):63.
9. Sun SN, Motta M, Tazhigulov RN, et al. Quantum computation of finite-temperature static and dynamical properties of spin systems using quantum imaginary time evolution. PRX Quantum. 2021;2(1):010317.
10. Motta M, Sun C, Tan ATK, et al. Determining eigenstates and thermal states on a quantum computer using quantum imaginary time evolution. Nat Phys. 2020;16(2):205–10.
11. Gomes N, Zhang F, Berthusen NF, et al. Efficient step-merged quantum imaginary time evolution algorithm for quantum chemistry. J Chem Theory Comput. 2020;16(10):6256–66.
12. Kosugi T, Nishiya Y, Nishi H, et al. Imaginary-time evolution using forward and backward real-time evolution with a single ancilla: first-quantized eigensolver algorithm for quantum chemistry. Phys Rev Res. 2022;4(3):033121.
13. Lin SH, Dilip R, Green AG, et al. Real-and imaginary-time evolution with compressed quantum circuits. PRX Quantum. 2021;2(1):010342.
14. Liu T, Liu JG, Fan H. Probabilistic nonunitary gate in imaginary time evolution. Quantum Inf Process. 2021;20(6):204.
15. Jouzdani P, Johnson CW, Mucciolo ER betal. Alternative approach to quantum imaginary time evolution. Phys Rev A. 2022;106(6):062435.
16. Cao C, An Z, Hou SY, et al. Quantum imaginary time evolution steered by reinforcement learning. Commun Phys. 2022;5(1):57.
17. Leadbeater C, Fitzpatrick N, Ramo DM, et al. Non-unitary Trotter circuits for imaginary time evolution. 2023. arXiv preprint. arXiv:2304.07917.
18. White SR. Minimally entangled typical quantum states at finite temperature. Phys Rev Lett. 2009;102(19):190601.
19. McClean JR, Parkhill JA, Aspuru-Guzik A. Feynman's clock, a new variational principle, and parallel-in-time quantum dynamics. Proc Natl Acad Sci. 2013;110(41):E3901–9.
20. McClean JR, Aspuru-Guzik A. Clock quantum Monte Carlo technique: an imaginary-time method for real-time quantum dynamics. Phys Rev A. 2015;91(1):012311.
21. Kamakari H, Sun SN, Motta M, et al. Digital quantum simulation of open quantum systems using quantum imaginary-time evolution. PRX Quantum. 2022;3(1):010320.
22. Okuma N, Nonnormal NYO. Hamiltonian dynamics in quantum systems and its realization on quantum computers. Phys Rev B. 2022;105(5):054304.
23. Al-Saidi WA, Zhang S, Krakauer H. Auxiliary-field quantum Monte Carlo calculations of molecular systems with a Gaussian basis. J Chem Phys. 2006;124(22):224101.
24. Motta M, Zhang S. Ab initio computations of molecular systems by the auxiliary-field quantum Monte Carlo method. Wiley Interdiscip Rev Comput Mol Sci. 2018;8(5):e1364.
25. Chan GKL, Sharma S. The density matrix renormalization group in quantum chemistry. Annu Rev Phys Chem. 2011;62:465–81.
26. Stoudenmire EM, White SR. Sliced basis density matrix renormalization group for electronic structure. Phys Rev Lett. 2017;119(4):046401.
27. Komsa HP, Krasheninnikov AV. Effects of confinement and environment on the electronic structure and exciton binding energy of MoS2 from first principles. Phys Rev B. 2012;86(24):241201.
28. Feynman RP. Simulating physics with computers. Int J Theor Phys. 2018;21(6/7):467–88.
29. Buluta I, Nori F. Quantum simulators. Science. 2009;326(5949):108–11.
30. Cirac JI, Zoller P. Goals and opportunities in quantum simulation. Nat Phys. 2012;8(4):264–6.
31. Georgescu IM, Ashhab S, Nori F. Quantum simulation. Rev Mod Phys. 2014;86(1):153.
32. Nielsen MA, Chuang IL. Quantum computation and quantum information. Cambridge: Cambridge University Press; 2010.
33. Beach MJS, Melko RG, Grover T, et al. Making trotters sprint: a variational imaginary time ansatz for quantum many-body systems. Phys Rev B. 2019;100(9):094434.
34. Koch M, Schaudt O, Mogk G, et al. A variational ansatz for Taylorized imaginary time evolution. ACS Omega. 2023;8(25):22596–602.
35. McClean JR, Romero J, Babbush R, et al. The theory of variational hybrid quantum-classical algorithms. New J Phys. 2016;18(2):023023.
36. Peruzzo A, McClean J, Shadbolt P, et al. A variational eigenvalue solver on a photonic quantum processor. Nat Commun. 2014;5(1):4213.
37. Yeter-Aydeniz K, Siopsis G, Pooser RC. Scattering in the Ising model with the quantum Lanczos algorithm. New J Phys. 2021;23(4):043033.
38. Yeter-Aydeniz K, Moschandreou E, Siopsis G. Quantum imaginary-time evolution algorithm for quantum field theories with continuous variables. Phys Rev A. 2022;105(1):012412.
39. Nishi H, Hamada K, Nishiya Y, et al. Analyzing computational cost of probabilistic imaginary-time evolution method. 2023. arXiv preprint. arXiv:2305.04600.

40. Wen J, Zheng C, Huang Z, et al. Iteration-free digital quantum simulation of imaginary-time evolution based on the approximate unitary expansion. Europhys Lett. 2023;141(6):68001.
41. Xie HN, Wei SJ, Yang F, et al. A Probabilistic Imaginary Time Evolution Algorithm Based on Non-unitary Quantum Circuit. 2022. arXiv preprint. arXiv:2210.05293.
42. Silva TL, Taddei MM, Carrazza S, et al. Fragmented imaginary-time evolution for early-stage quantum signal processors. 2021. arXiv preprint. arXiv:2110.13180.
43. Long GL. General quantum interference principle and duality computer. Commun Theor Phys. 2006;45(5):825.
44. Wei SJ, Long GL. Duality quantum computer and the efficient quantum simulations. Quantum Inf Process. 2016;15:1189–212.
45. Yi X, Huo JC, Gao YP, et al. Iterative quantum algorithm for combinatorial optimization based on quantum gradient descent. Results Phys. 2024;56:107204.
46. Trotter HF. On the product of semi-groups of operators. Proc Am Math Soc. 1959;10(4):545–51.
47. Suzuki M. Generalized Trotter's formula and systematic approximants of exponential operators and inner derivations with applications to many-body problems. Commun Math Phys. 1976;51(2):183–90.
48. Li K, Wei S, Gao P, et al. Optimizing a polynomial function on a quantum processor. npj Quantum Inf. 2021;7(1):16.
49. McArdle S, Endo S, Aspuru-Guzik A, et al. Quantum computational chemistry. Rev Mod Phys. 2020;92(1):015003.
50. Hehre WJ, Ditchfield R, Pople JA. Self-consistent molecular orbital methods. XII. Further extensions of Gaussian-type basis sets for use in molecular orbital studies of organic molecules. J Chem Phys. 1972;56(5):2257–61.
51. Wei S, Li H, Long GL. A full quantum eigensolver for quantum chemistry simulations. Research. 2020.
52. Colless JI, Ramasesh VV, Dahlen D, et al. Computation of molecular spectra on a quantum processor with an error-resilient algorithm. Phys Rev X. 2018;8(1):011021.
53. Bose S. Quantum communication through an unmodulated spin chain. Phys Rev Lett. 2003;91(20):207901.
54. Nishi H, Kosugi T, Nishiya Y, et al. Acceleration of probabilistic imaginary-time evolution method combined with quantum amplitude amplification. 2022. arXiv preprint. arXiv:2212.13816.
55. Babbush R, McClean J, Wecker D, et al. Chemical basis of Trotter-Suzuki errors in quantum chemistry simulation. Phys Rev A. 2015;91(2):022311.
56. Childs AM, Maslov D, Nam Y, et al. Toward the first quantum simulation with quantum speedup. Proc Natl Acad Sci. 2018;115(38):9456–61.
57. Childs AM, Ostrander A, Su Y. Faster quantum simulation by randomization. Quantum. 2019;3:182.

Publisher's note